nature communications

Article

https://doi.org/10.1038/s41467-025-62538-8

Personalized ML-based wearable robot control improves impaired arm function

Received: 5 December 2024

Accepted: 18 July 2025

Published online: 02 August 2025

Check for updates

James Arnold[1,5], Prabhat Pathak[1,5], Yichu Jin[1], David Pont-Esteban[1], Connor M. McCann[1], Carolin Lehmacher[1], John P. Bonadonna[1], Tanguy Lewko[1], Katherine M. Burke[2], Sarah Cavanagh[1,3,4], Lynn Blaney[3], Kelly Rishe[3,4], Tazzy Cole[1], Sabrina Paganoni[2], David Lin[3,4] & Conor J. Walsh[1]

Portable wearable robots offer promise for assisting people with upper limb disabilities. However, movement variability between individuals and trade-offs between supportiveness and transparency complicate robot control during real-world tasks. We address these challenges by first developing a personalized ML intention detection model to decode user's motion intention from IMU and compression sensors. Second, we leverage a physics-based hysteresis model to enhance control transparency and adapt it for practical use in real-world tasks. Third, we combine and integrate these two models into a real-time controller to modulate the assistance level based on the user's intention and kinematic state. Fourth, we evaluate the effectiveness of our control strategy in improving arm function in a multi-day evaluation. For 5 individuals post-stroke and 4 living with ALS wearing a soft shoulder robot, we demonstrate that the controller identifies shoulder movement with 94.2% accuracy from minimal change in the shoulder angles (elevation: 3.4°, depression: 1.7°) and reduces arm-lowering force by 31.9% compared to a baseline controller. Furthermore, the robot improves movement quality by increasing their shoulder elevation/depression (17.5°), elbow (10.6°) and wrist flexion/extension (7.6°) ROMs; reducing trunk compensation (up to 25.4%); and improving hand-path efficiency (up to 53.8%).

Upper limb motor impairment, either due to injury such as stroke or neurodegenerative diseases such as amyotrophic lateral sclerosis (ALS), impedes functional use of the arm in daily life. Recently, a number of portable, wearable robots have been developed to augment the residual movement of individuals with upper limb impairments[1–3]. Our group previously presented an inflatable, wearable shoulder robot with a controller that used inertial measurement unit (IMU)-estimated joint angles and velocities to dynamically assist upper limb movements by offloading the weight of the arm[3]. We chose to offload the weight of the arm around the shoulder, the largest torque-bearing upper limb joint, since gravity offloading is known to decrease the burden on the damaged nervous system, thereby reducing abnormal joint movement and leading to improvement in functional tasks[4–6]. However, high inter-individual variability in residual movement[7] creates a challenge for effective wearable robot control, especially during functional tasks.

For intuitive control of a wearable robot, accurate detection of motion intention is critical. Prior work has considered a number of non-invasive, privacy-preserving, and automated approaches to detecting a user's intention. Surface electromyography (sEMG) sensors are the most common sensing modality for intention recognition in

[1]John A. Paulson School of Engineering and Applied Sciences, Harvard University, Cambridge, MA, USA. [2]Neurological Clinical Research Institute, Massachusetts General Hospital, Boston, MA, USA. [3]Center for Neurotechnology and Neurorecovery, Department of Neurology, Massachusetts General Hospital, Boston, MA, USA. [4]Department of Veterans Affairs, Rehabilitation Research and Development Service, Providence, RI, USA. [5]These authors contributed equally: James Arnold, Prabhat Pathak. e-mail: walsh@seas.harvard.edu

both wearable robots[8] and robotic prostheses[9]. The sEMG sensors are used due to their utility in detecting anticipatory movement intention[10], as electrical activity in the muscles precedes joint movement, potentially reducing the latency between the detection of movement intention and the application of assistive forces. Early work in intention detection[11,12] focused on low-latency EMG decoding for prosthetic control but did not integrate decoding with actuation. Recent work has advanced evaluation of intention detection models by testing models within target systems[13] and evaluating sEMG performance across multiple days[14]. However, the sEMG sensors used in these prior works have practical challenges such as requiring precise placement on the skin, maintaining a stable skin-electrode interface, and lacking robustness to sweat. For example, the MyoPro powered elbow and hand orthosis from Myomo uses sEMG for control but requires a trained professional for the initial placement of sEMG electrodes and tuning sEMG onset thresholds[15]. These limitations pose practical challenges for a person with upper limb impairments to use a wearable robot independently and across days.

Alternative wearable sensors that could potentially mitigate the usability challenges associated with sEMG are IMUs and force/compression sensors. IMU-estimated kinematic information has been used to decode intention from user motion, primarily through thresholding and proportional or functional mapping of joint angles or velocities to output actuation[16–18]. In addition, force sensors that monitor the loads exerted on the body have also been explored, though primarily for non-portable and/or rigid upper limb devices or hand devices[19–21].

A wearable robot controller also requires a model of the relationship between the commanded actuation and its effect on the human-robot system. Modeling this relationship is often non-trivial, since this relationship is typically hysteretic[3,22] because of textile components common in wearable robots. Model inaccuracies can make a robot ineffective or unusable for impaired users who cannot easily compensate for over-/under-assistance. Recently, our group introduced a practical hysteresis modeling approach that can be personalized to each user of wearable robots[23]. This model was shown to minimize the potential for applying incorrect levels of assistance compared to more commonly used, simpler curve-fitting models. However, this model has yet to be integrated into any closed loop controller, and its effectiveness for assisting those with upper limb impairments has not yet been tested.

Past studies of wearable robots for individuals with upper limb impairments have focused on evaluating the reduction in muscle activity[24], range of motion of at least one joint[1], or changes in clinical scores[25]. In a recent study with our soft wearable shoulder robot[3], we presented an evaluation approach that used tasks ranging from single joint movements to functional tasks requiring arm elevation to assess changes in the movement quality of the shoulder and trunk using a soft wearable robot. While we assessed changes in the movement quality of the shoulder and trunk during lifting, we did not evaluate changes in the distal joint and hand movement quality over the full range of arm movement, i.e., lifting and lowering. This is important as previous studies have emphasized that an adequate level of movement quality for all the joints in the upper limb kinematic chain over the full range of gross arm movement is necessary to effectively perform functional tasks[26,27].

The objective of this research is to develop an intention-based control strategy for an inflatable soft wearable robot to assist the shoulder of individuals with various upper limb impairments. We achieve this by first developing a machine learning (ML) intention detection model to infer arm motion from kinematic and human-robot interaction information captured using IMUs and custom soft compression sensors, respectively. Second, we introduce a method that leverages the human-robot system's inherent hysteresis using a physics-based model to estimate the minimum pressure needed to support the arm and ensure transparency during lowering. Third, we present a real-time control approach that combines the intention detection and physics-based hysteresis models that can run onboard the portable robot to adaptively control the assistance level based on the user's motion intention and kinematic state. Finally, we evaluate the controller's effectiveness in improving overall arm function through previously unseen tasks involving isolated and functional movements in individuals post-stroke and with ALS, through in-lab assessment and at-home demonstration.

Results

Overview of soft wearable robot and control strategy

To support the impaired shoulder movement of individuals post-stroke and living with ALS, we advanced the sensing capabilities of a soft wearable robot that provides support with an inflatable actuator under their impaired arm (Fig. 1A). Specifically, in addition to using inertial measurement units, we integrated custom soft compression sensors whose combined data could be used as control inputs to sense the participants' residual movement (Fig. 1B). The custom compression sensors are textile-based soft capacitors that measure changes in sensor thickness during human-robot interaction, which correlate to the compression force applied to the sensor (Supplementary Fig. S1).

Trained from guided sessions (Fig. 1C, Supplementary Table S1) requiring on average 17:04 ± 3:26 (minutes:seconds) to perform, personalized intention detection models (IDMs) could classify the intended direction of shoulder movement–UP, DOWN, or HOLD–for 5 individuals post-stroke and 4 individuals living with ALS. For each participant, the IDM was combined with a physics-based model which captured the hysteretic mapping from the shoulder elevation angle to the actuator pressure necessary for anti-gravity support. Specifically, the IDM classifications were used to offset input angles to the hysteresis model to rapidly promote shoulder elevation/depression movement or gradually approach the estimated minimum necessary level of support to maintain a constant shoulder elevation. We modeled this hysteresis with a Preisach model[23] (Supplementary Fig. S2) based on data from three cyclical inflation/deflation cycles of decreasing magnitude (Fig. 1D) while the participant was instructed to keep their arm limp.

Development and evaluation of personalized motion intention detection models

We evaluated the IDM accuracy during an evaluation session where the IDM real-time predictions (100 Hz) were used for the robot's control as participants performed joint individuation ($n = 9$) and simulated functional tasks ($n = 8$, excluding one participant living with ALS who could not complete the tasks due to fatigue). We evaluated the UP/DOWN classes during cued shoulder lifting/lowering movements and the HOLD class during other cued movements where participants were instructed to maintain steady shoulder elevation (Fig. 2A). We chose to evaluate the HOLD class only during simultaneous volitional movement since, compared to static holding, this scenario is more challenging to classify and more akin to functional use.

Accuracy was defined according to a comparison of the real-time IDM predictions and the ground truth intention labels assigned from the movement cues. Specifically, we defined correctly classified movements as those where the plurality of real-time IDM class predictions was correct (Supplementary Fig. S3A). This way, we could separate between movements that were predominately classified correctly versus those with longer periods of misclassified timesteps which have a greater impact on the control. However, movements designated as misclassified can still contain periods of time where the real-time IDM predictions are correct. In fact, across all participants and tasks, the participants' intention was identified for a sufficient period of time to trigger actuation.

We found that, on average, the accuracy of the IDMs was 94.2 ± 2.0% across the nine participants, corresponding to 93.6 ± 9.1%,

https://doi.org/10.1038/s41467-025-62538-8

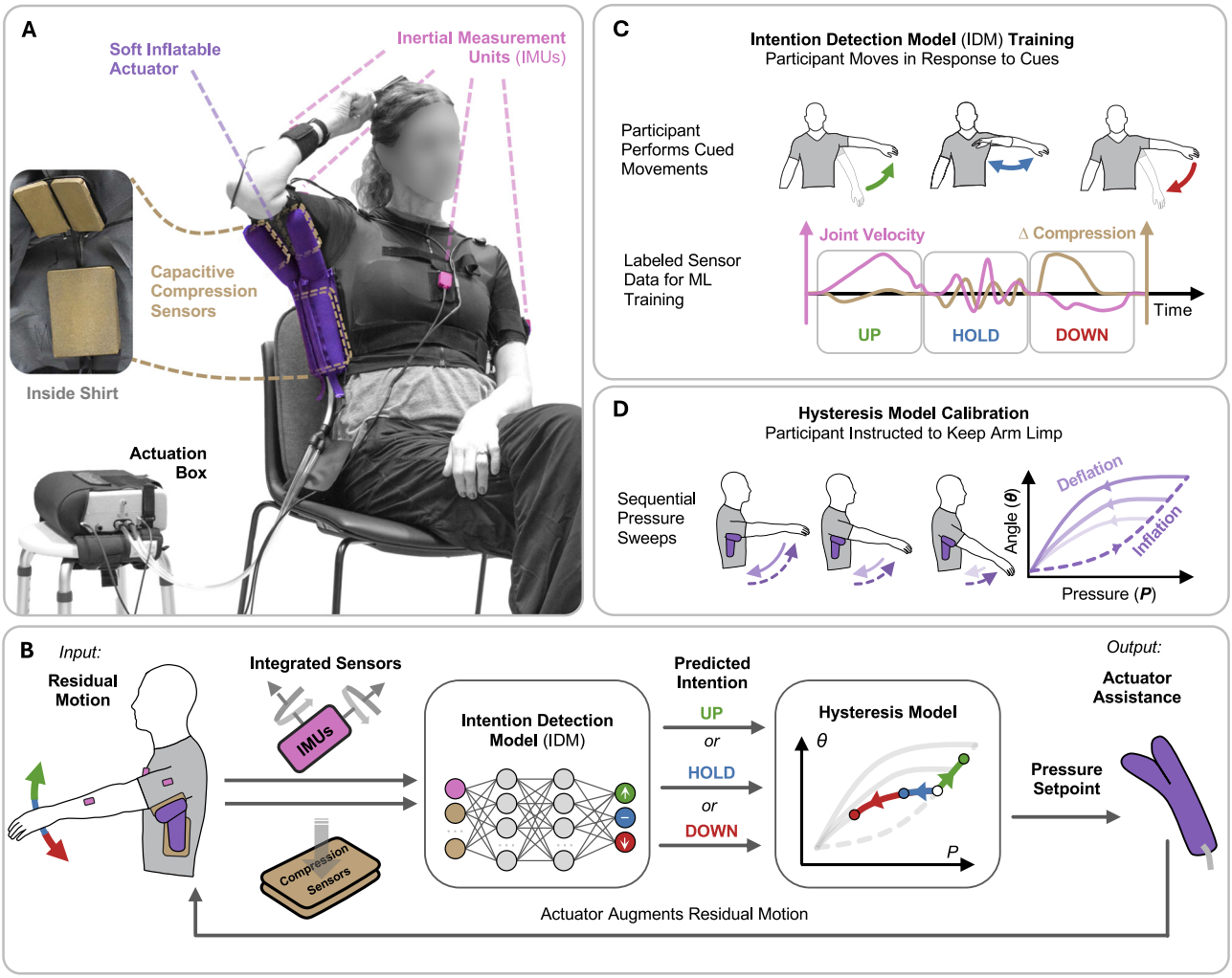

Fig. 1 | Overview of the soft wearable robot and high-level control strategy. **A** The components of the soft wearable robot that provides shoulder assistance using an inflatable actuator. The robot has integrated IMUs and soft compression sensors. All the electronics, valves, fluidic supply, and batteries used to power and control the robot are housed in a portable actuation box that can be worn at the waist or positioned beside the user. **B** Real-time controller designed to augment residual motion by combining a personalized intention detection model (IDM) and hysteresis model. Wearable sensors captured residual arm movements which were classified by the IDM. The real-time intention classification determined the target elevation angle, and the hysteresis model determined the pressure necessary to achieve this target angle. **C** IDM training data collection overview (performed only once per participant and not re-trained for subsequent days). Participants were instructed to perform a variety of upper limb movements to collect IMU and compression sensor data labeled based on the instructed shoulder elevation: lifting the arm (UP), maintaining the arm elevation (HOLD), and lowering the arm (DOWN). **D** Hysteresis model calibration procedure (performed each time the robot is donned). Each participant was instructed to keep their arm limp while the actuator swept the pressure.

93.0 ± 6.4%, and 96.1 ± 4.3% for UP, HOLD, and DOWN, respectively (Fig. 2B). In the context of the IDMs' use for robot control, misclassified movements manifested as either delayed or discontinuous actuation for UP and DOWN or perturbations in the robot-provided support during HOLD. The specific effects of IDM misclassifications are presented in the subsequent section on the integrated controller.

To assess the quality of the accuracy results, we compared this group accuracy (where each participant's evaluation data was classified by their own personalized model) to accuracies found in post-processing (where all participants' evaluation data were classified by all other models and a generalized model trained from all participants' data). We found that having a personalized IDM for each participant enabled the highest accuracy across the group, least misclassifications, and lowest standard deviation among inter-participant accuracies (Supplementary Table S2). A generalized IDM (trained on all participants' data) achieved an accuracy of 87.2 ± 5.8% which was 7.5% lower than the group accuracy for personalized IDMs.

Furthermore, we assessed the personalized IDMs' responsiveness in terms of time and angle to the first identification of UP and DOWN intention (Fig. 2E). We found that the time until the first correct prediction of UP and DOWN was 218 ± 206 ms and 178 ± 123 ms, respectively, from the video labeled initiation time. These times correspond to small changes in shoulder elevation (estimated from optical motion capture) before intention was first predicted by the IDMs: 3.4 ± 2.0° shoulder elevation and 1.7 ± 2.2° shoulder depression for UP and DOWN, respectively. Given that the average change in shoulder elevation was 11.5 ± 4.4° within each cued HOLD movement, the small displacements required to trigger UP/DOWN predictions imply the IDMs could reliably distinguish between wearable sensor signal changes caused by voluntary changes in shoulder elevation as compared to changes caused by involuntary movements.

Controlling the robot with user intention detection models

Supplementary Fig. S4 shows the robot controller that was designed to enable real-time assistance and transparent user-directed movement.

https://doi.org/10.1038/s41467-025-62538-8

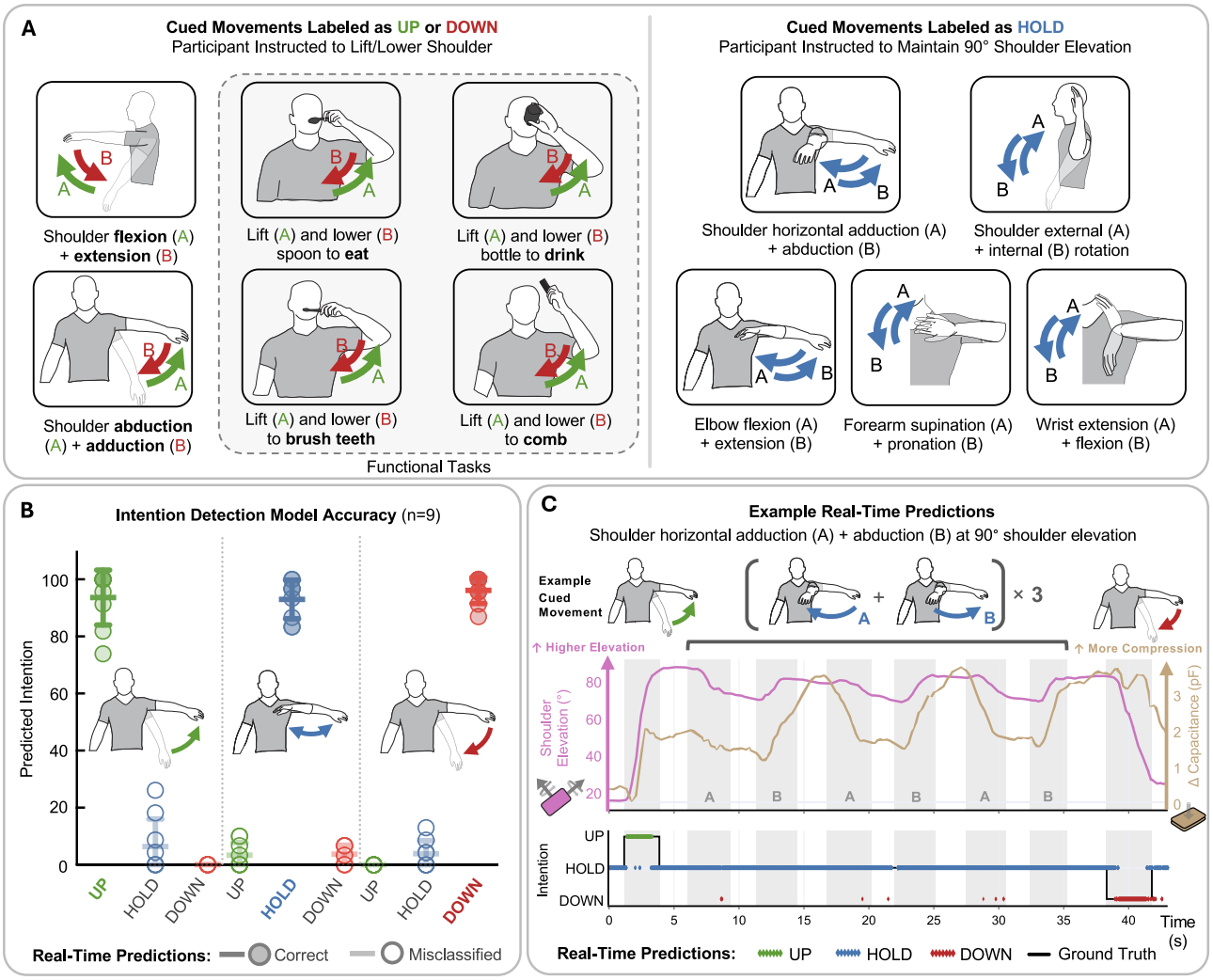

Fig. 2 | Evaluation of intention detection models on unseen movement data. **A** The cued movements participants performed to evaluate their personalized IDMs. This evaluation was performed on a separate day from the IDM training to demonstrate that the personalized IDMs do not need to be re-trained each time the robot is donned. **B** IDM accuracy/confusion for the nine participants across the movements (for one participant, functional tasks were excluded). Each colored bar represents the mean percentage of movements predicted to be a particular class (±standard deviation), grouped by the correct class. Overlaid points show individual participant data. **C** *Top:* Representative sensor data showing IMU-estimated elevation angle (pink, left y-axis) and average change in compression (gold, right y-axis). *Bottom:* IDM real-time predictions from one participant during the shoulder elevated horizontal abduction/adduction task.

Rather than always querying the human-robot hysteresis model to find the necessary pressure to support the gravitational load of the arm in its current pose (i.e., pure gravity compensation), the controller predicted the pressure required for future states based on the IDM-predicted direction of intention (Fig. 3A). In the UP and DOWN states, the measured elevation angle was (optionally) offset by a constant angle in the direction of movement, allowing the robot to anticipate and promote a user's future movement in that direction. In the HOLD state, the controller's objective was to maintain antigravity support while maximizing the transparency of the system (i.e., at the minimum actuator pressure). Given the typical shape of the hysteretic curves for our system, the actuator pressure could be reduced significantly in the HOLD state while still maintaining support of the arm (Fig. 3A, middle). Animations of the controller response time synchronized with videos of participants performing functional and joint individuation tasks are presented in Supplementary Movie 1.

We evaluated the actuator pressure response to assess how reactive the controller was when a user intended to change their shoulder elevation. These times to actuation include the contributions of the IDM, hysteresis model, low level pressure controller, and fluid dynamics. Across all UP movements, the average time and shoulder elevation angle until measured actuator inflation due to a UP intention model prediction was 498 ± 150 ms and 13.0 ± 4.2°, respectively (Fig. 3C, left). Across all DOWN movements, the average time and shoulder depression angle until measured actuator deflation due to a DOWN intention model prediction was 378 ± 115 ms and 6.7 ± 5.3°, respectively (Fig. 3C, right). IDM UP/DOWN misclassifications manifested as delayed actuation, with UP and DOWN misclassification times to actuation of 1024 ± 1030 ms and 569 ± 586 ms, respectively.

We validated the hysteresis model's ability to predict the minimum necessary pressure during HOLD by evaluating the change in angle during the steady elevation at 90° portion of the isolated shoulder flexion and abduction tasks ($n = 9$). A representative figure of the controller response during the isolated shoulder abduction task is shown in Fig. 3B. During the period when participants were instructed to keep their shoulder elevated, the actuator pressure dropped by 16.7 ± 10.4 kPa (16.1 ± 10.0% of the range of possible commanded pressure) on average across the 9 participants. However, the shoulder depressed, on average, by only 1.7 ± 1.9°, demonstrating that the actuator maintained support of the arm. The high standard deviation of pressure dropped is reflective of the user-specific hysteresis calibrations. Depending on the fit of the shirt and arm weight, the shape of

https://doi.org/10.1038/s41467-025-62538-8

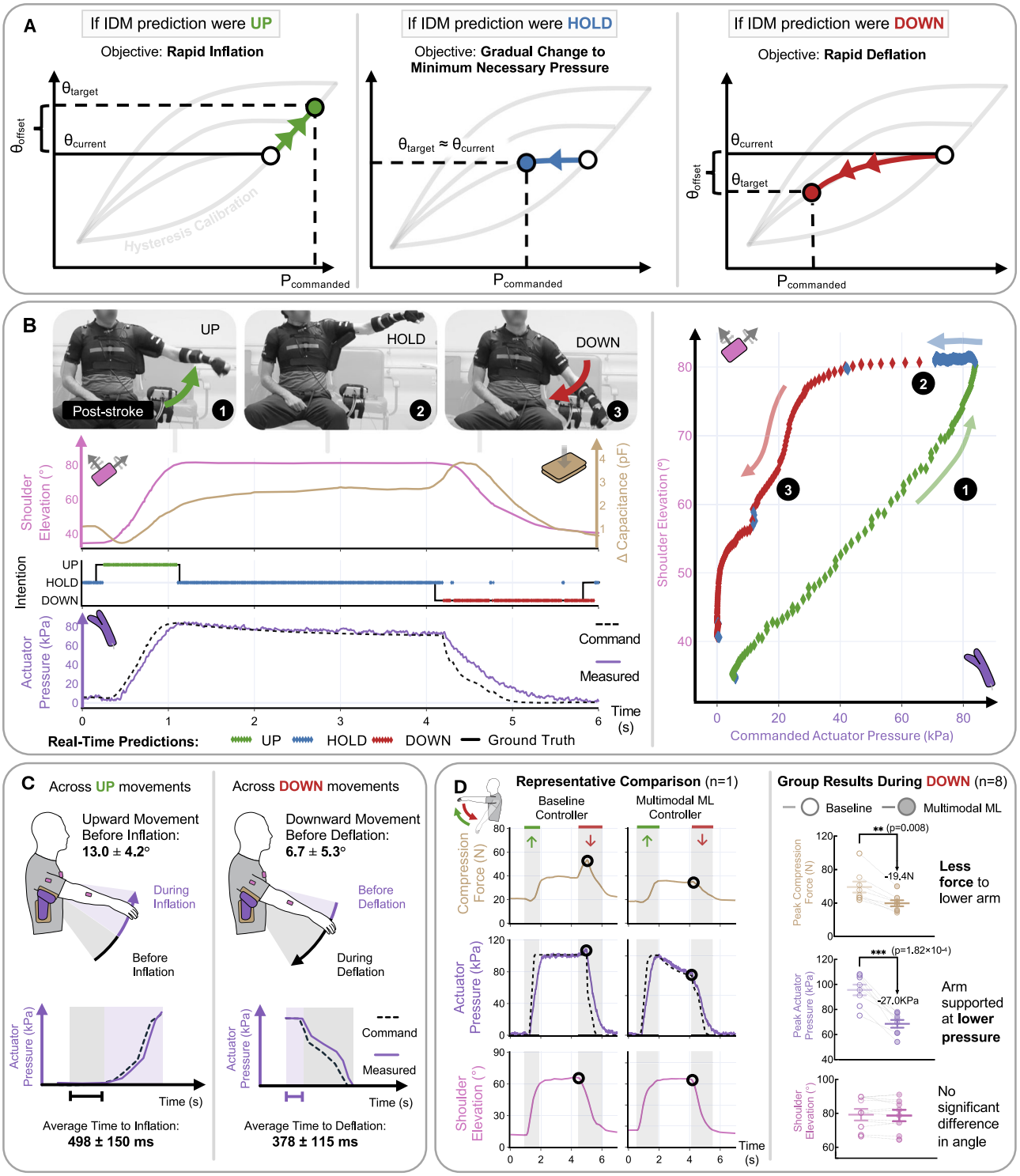

Fig. 3 | Control objectives and real-time controller performance. A Control objectives during the three intention states. Arrows show the commanded pressure trajectory from the initial (white circle) to target state (colored circle) based on the predicted intention and hysteresis calibration (gray). **B** Example shoulder abduction/adduction response. Left: time series of shoulder elevation (pink), mean compression change (gold), IDM-predicted intention (diamonds), ground truth (black), and actuator pressure (measured, purple; commanded, dashed black). Right: elevation vs. commanded pressure, colored by intention. **C** Responsiveness results across participants ($n = 9$). **D** Representative time series ($n = 1$ participant post-stroke, left) and group ($n = 8$, right) results showing the differences in force (estimated from compression sensors), actuator air pressure, and shoulder elevation between baseline gravity compensation control and multimodal ML control during shoulder extension and adduction. Two-tailed paired t-tests or Wilcoxon signed-rank tests assessed statistical significance; lines and error bars indicate means ± standard errors.

Table 1 | Participant cohort

Participant	Cause of impairment	Shoulder supported	Sex	Dominant arm	Shirt size	Clinical score
P1	Stroke	L	M	R	L	FMA-UE: 35/60
P2	Stroke	L	M	L	XL	FMA-UE: 31/60
P3	Stroke	L	M	R	XL	FMA-UE: 55/60
P4	Stroke	L	M	L	M	FMA-UE: 31/60
P5	Stroke	L	M	R	L	FMA-UE: 53/60
P6	ALS	L	F	R	L	ALSFRS-R: 33/48
P7	ALS	R	F	R	S	ALSFRS-R: 37/48
P8	ALS	R	F	R	XL	ALSFRS-R: 35/48
P9	ALS	L	F	R	L	ALSFRS-R: 43/48

Upper Limb Fugl-Meyer Assessment (FMA-UE) out of 60 (motor function subscore without reflexes) and Revised ALS Functional Rating Scale (ALSFRS-R) out of 48.

the deflation curves was different and allowed for a different level of pressure drop to maintain support. The minimum necessary pressure response was also observed during functional tasks (Supplementary Fig. S5).

IDM misclassifications during HOLD–78.9% of which occurred during shoulder elevated internal/external rotation–manifested as perturbations in the applied pressure. Across participants' misclassified HOLD movements, an average 5.9 ± 9.2° decrease and 6.7 ± 10.3° increase in elevation angle were measured during movements misclassified as DOWN and UP, respectively. Despite these misclassification-induced perturbations, the robot was observed to have a stabilizing effect on the user's shoulder elevation even during misclassifications, and the controller addressed misclassifications by slowly inflating or deflating back to the estimated minimum pressure required for support (Supplementary Fig. S6).

We evaluated the controller's ability to enable transparent arm lowering by comparing our proposed multimodal ML controller to a baseline controller that performs pure kinematic-based gravity compensation[23] with the user-specific hysteresis model (i.e., there is no intention information incorporated from an IDM in the baseline controller). A representative comparison of these conditions during one repetition of isolated shoulder flexion/extension is shown in Fig. 3D. There was a notable reduction in the amount of force required for the participants to lower their arms when using the multimodal ML controller. From the compression sensor on the torso, we estimate that the multimodal ML controller reduced the peak lowering force during DOWN by 19.4 ± 3.3 N (−31.9 ± 2.6%, $p = 0.008$) across 8 participants (Supplementary Fig. S1). Also, the peak measured actuator pressure during DOWN was 27.0 ± 3.8 kPa (−27.8 ± 3.2%, $p = 1.82\times10^{-4}$) lower despite there being no significant difference in initial angle estimated by the IMUs at the start of DOWN. One participant living with ALS was excluded from this analysis since they were only able to perform the task with the multimodal ML controller and could not trigger inflation with the baseline controller during the evaluation session.

Improvement in upper limb function and movement quality

We evaluated the efficacy of the soft wearable robot with the proposed controller in improving the upper limb movement quality for 9 participants (5 individuals post-stroke and 4 living with ALS) during joint individuation and for 8 participants during functional tasks (See "Experimental procedure for evaluation"). The characteristics of the participants are provided in Table 1. We calculated the range of motion of the shoulder, elbow, and wrist joints to evaluate joint function. Additionally, we calculated three-dimensional (3D) trunk center of mass (COM) displacement to evaluate trunk compensation, and calculated hand-path-ratio (HPR) and spectral arc length (SPARC) of 3D hand COM trajectory to evaluate hand path efficiency and smoothness (See "Upper limb Movement Quality"). We also evaluated the effect of the robot on the upper limb movement quality metrics separately for the two participant subgroups based on the cause of impairment (Stroke and ALS) and compared robot-induced changes in movement quality for the two groups (See "Upper limb Movement Quality"). The soft wearable robot improved joint function, decreased trunk compensation, and increased hand path efficiency across 9 participants during individuation and across 8 participants during functional tasks.

The robot significantly increased shoulder elevation/depression ROM (+17.5 ± 4.6°, $p = 0.004$), elbow (+10.6 ± 2.4°, $p = 0.002$), and wrist (+7.6 ± 2.8°, $p = 0.026$) flexion/extension ROM during individuation tasks (Fig. 4A). However, the robot did not yield significant differences in shoulder horizontal abduction/adduction and internal/external rotation, and forearm supination/pronation ROMs during individuation tasks (Supplementary Table S7). The robot also significantly reduced trunk compensation by decreasing trunk COM displacement only during DOWN direction movement for the individuation task (−25.4 ± 6.2%, $p = 0.009$). In addition, the trunk COM displacement significantly decreased during both movement directions for the functional task (UP: −11.9 ± 3.9%, $p = 0.014$; DOWN: −12.9 ± 4.6%, $p = 0.016$) (Fig. 4B). Finally, the robot improved hand movement efficiency by significantly decreasing HPR for both individuation (UP: −43.1 ± 8.4%, $p = 0.019$; DOWN: −53.8 ± 10.2%, $p = 0.018$) and functional (UP: −22.2 ± 3.6%, $p = 0.008$; DOWN: −22.1 ± 2.6%, $p = 0.008$) tasks (Fig. 4C). However, the robot did not yield significant changes in smoothness (Supplementary Table S7).

A comparison of robot-induced improvement in movement quality between participant subgroups revealed that the improvements in joint function were significantly higher for individuals living with ALS than post-stroke. Combining the tasks where the ROM significantly increased across the 9 participants, we found that while the robot significantly increased these ROMs for the Stroke (+6.4 ± 1.1°, $p = 5.80\times10^{-5}$) and ALS (+18.8 ± 3.5°, $p = 2.55\times10^{-4}$) subgroups, the magnitude of improvement was significantly larger for ALS than the magnitude for Stroke ($p = 0.005$) (Fig. 4D). Performing this subgroup-separate analysis for tasks where ROM did not significantly change across the 9 participants, we found that the robot significantly increased the ROMs only for the ALS subgroup (+9.9 ± 2.7°, $p = 4.88\times10^{-4}$), and the magnitude of improvement was significantly larger for ALS than magnitude for Stroke ($p = 4.28\times10^{-5}$). Lastly, combining the values of trunk compensation and hand movement related metrics for individuation and functional tasks, we found that the robot significantly reduced trunk COM displacement (Stroke: −12.6 ± 3.0%, $p = 1.05\times10^{-4}$; ALS: −18.6 ± 6.0%, $p = 0.005$) and HPR (Stroke: −29.0 ± 4.8%, $p = 3.62\times10^{-5}$; ALS: −46.2 ± 6.9%, $p = 1.22\times10^{-4}$) separately for each subgroup (Fig. 4E). However, no significant differences were observed in percent improvement in these metrics between the two subgroups, indicating that the robot provides similar benefit in reducing trunk compensation and hand path efficiency for the ALS and Stroke subgroups.

https://doi.org/10.1038/s41467-025-62538-8

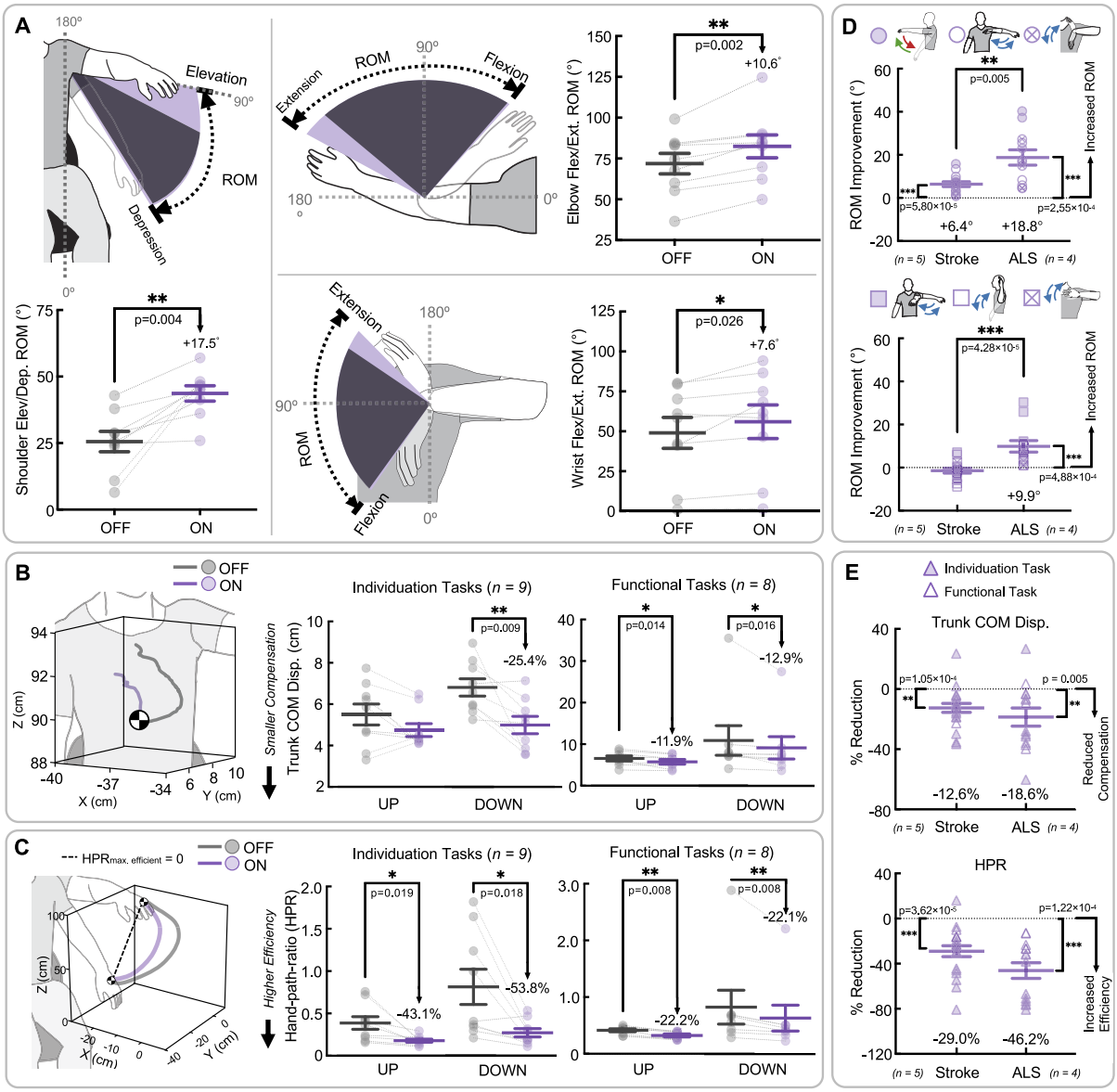

Fig. 4 | Improved upper limb function and movement quality with multimodal ML control of the soft wearable robot. A Representative illustration, and the results of the comparison of shoulder elevation/depression, and elbow and wrist flexion/extension range of motions (ROMs) during individuation ($n = 9$) tasks under two conditions: robot turned off (OFF; gray shaded region and line with error bars) and turned on (ON; purple shaded region and line with error bars). **B** Representative illustration and results of comparisons of the three-dimensional (3D) trunk center of mass (COM) displacement during individuation ($n = 9$) and functional tasks ($n = 8$) under OFF and ON conditions. **C** Representative illustration of 3D hand COM trajectory and results of comparison of mean hand-path-ratio (HPR) during individuation tasks and functional tasks under OFF and ON conditions. In **A**–**C**, two-tailed paired t-test or Wilcoxon-signed rank tests were used to evaluate significant differences in all the movement quality metrics between ON and OFF, and the line and error bars are the mean and standard error. **D** The comparison of significantly improved ROMs and not significantly different ROMs between the two participant groups, individuals post-stroke ($n = 5$) and living with ALS ($n = 4$), and separately between ON and OFF for each group. **E** The comparison of trunk COM displacement and HPR between two participant groups and separately between ON and OFF for each group. In (**D**, **E**), significant differences in movement quality between the groups were performed using independent t-test or Mann–Whitney U tests, and between ON and OFF were performed using two-tailed paired t-test or Wilcoxon-signed rank tests. The purple line and error bars in (**D** and **E**) are the mean and standard error of the improvements compared to OFF condition. Overlaid points show individual participant data. ***($p < 0.001$), **($p < 0.01$) and *($p < 0.05$) denotes statistically significant difference.

At-home demonstration

We evaluated the robot's performance in real-world, at-home settings to better understand its effectiveness during prolonged daily use and while interacting with weighted objects. To do this, we brought the robot to the homes of one participant post-stroke and one living with ALS, where they performed shoulder elevated, weight-holding tasks and activities of daily living (ADLs). Both participants held weights higher and longer with the multimodal ML controller enabled (Supplementary Fig. S8). At the elevated postures following abduction and flexion, shoulder elevation increased by 43.5 ± 13.0% and 53.5 ± 10.3% (Stroke) and by 33.7 ± 6.8% and 9.4 ± 5.8% (ALS), respectively. Task duration increased by 179.5% and 66.1% (Stroke) and by 65.7% and 30.7% (ALS), respectively. For the ADLs, we assessed controller performance before and after prolonged use involving repetitive joint

movement and weight-holding and found that the robot provided dynamic assistance throughout ADLs in all cases (Supplementary Fig. S9). However, we observed reduced mean pressure of support following self-reported fatigue in the ALS participant, highlighting a potential direction for future work on fatigue-adaptive control. Supplementary Movie 2 compiles videos of participants performing tasks with and without the assistance provided by the robot with the multimodal ML controller during the in-lab assessment and at-home demonstration.

Discussion

As wearable robots for those with upper limb impairments continue to become more portable and suitable for integration into unstructured environments, intuitive and reliable control will be critical for enabling functional arm use. Toward this goal, we developed and evaluated the effect of a control strategy that combines models of the human user's intention and human-robot hysteresis to control a soft inflatable shoulder robot in individuals with diverse types of upper limb motor impairments. We demonstrated that an ML model that uses a lightweight neural network could be trained from a short, guided session and then run in real-time to classify a user's intended shoulder elevation/depression. Furthermore, we showed that combining detected intention with a model of human-robot hysteresis allowed the controller to be both supportive and transparent. Finally, by systematically tracking all the upper limb joints and segment movements, we were able to demonstrate improvements in joint function and reductions in compensations for tasks ranging from single joint movement to functional activities.

A key innovation of our control strategy is leveraging personalized IDMs that combine IMUs and custom soft compression sensors to capture kinematics and human-robot interaction, respectively, to infer arm motion. By purposefully evaluating the control strategy over multiple days and on unseen tasks, we took into account the challenge of sensor misalignment across days and pathological involuntary movement not seen during the training of IDMs. Despite these challenges, we showed that the personalized IDMs identified the participants' intended direction of shoulder elevation in real-time with a high accuracy of 94.2 ± 2.0%. This compares to about 85% from sEMG only[28] and with multimodal sensor inputs[29] for hand movement classification of individuals post-stroke. Additionally, another study[2] used real-time muscular activity of upper limb muscles to classify between static holding and isolated shoulder and elbow flexion/extension movement for healthy adults with an average accuracy of 96.2%. Due to the differences in sensing modalities, detected movements, and/or study participant population, directly comparing our accuracy with results from existing literature is challenging. Still, unlike the single-degree of freedom simple motions detected in previous studies, we purposefully evaluated our intention detection model during multi-degree of freedom, complex motions where misclassifications were more likely to occur due to pathological involuntary movements and/or sensor misalignment.

We further evaluated the controller in terms of its response time to the users' volitional shoulder elevation/depression movements. We found that the IDMs took, on average, 218 ± 206 ms and 178 ± 123 ms to predict UP and DOWN intention, respectively. We also found the time to actuation was 498 ± 150 ms and 378 ± 115 ms for UP and DOWN, respectively. In prior works, the time to actuation has been calculated from the time to record and process sensor data[2,3], but these estimates do not include the intention detection performance or other potential sources of delay such as low-level controller response and actuator dynamics. Both the sensing and actuation methods we chose contribute to the overall actuation delay. While participants did not report issues with latency, we did not systematically assess user perception, which should be addressed in future work. We selected sensors that do not require precise placement or a stable skin interface and a lightweight, transparent actuation method to support multi-day usability. While IMU and force sensors have been shown to achieve comparable performance to sEMG sensors for intention detection[30], another study[31] demonstrated that sEMG sensors can offer faster detection than using interaction force. Alternative actuation methods, such as cable-driven or electromechanical systems, may further reduce latency compared to pneumatic systems and could be implemented with adaptations of the proposed control strategy.

Evaluated in prior work with clinical populations, mechanical transparency for soft wearable robots has been quantified by whether the robot restricts the users' ROM when the robot is unpowered[3,32]. However, the transparency when the robot is unpowered does not account for the potential effects of the force applied by the robot on the effort required by the user to move their joints. In this study, the custom soft compression sensors enabled real-time control and an assessment of this transparency. We combined the additional information provided by modeling human intention with a physics-based model that encapsulates the hysteresis of the inflatable actuator to predict the minimum actuator pressure to hold the arm. Integrating these models into a real-time controller, we demonstrated a significant reduction in effort to lower the arm compared to a baseline gravity compensation controller (31.9 ± 2.6% reduction in force). This result is likely enabled by both the controller's rapid deflation in DOWN and the reduced actuator pressure predicted by the hysteresis model during HOLD. Considering the improvements observed in joint function, this reduction in effort to lower the arm suggests that the controller maintains the robot's supportiveness while also being transparent when lowering the arm.

Our results and new control strategy can also provide insights into the potential assistive and rehabilitative applications of soft wearable robots. Previous studies have shown that upper limb impairments impede movement quality by reducing joint ROM, requiring greater trunk compensation to move the hand in 3D space[26,27,33]. The effectiveness of wearable and stationary in-clinic robots in reducing compensatory movement during isolated joint movements and reaching tasks has been demonstrated in the past studies[34–36]. In contrast, our robot enabled participants to move their arm with reduced trunk compensation during isolated joint movement and functional tasks that simulated activities of daily living (Fig. 4C). This indicates that the robot can curtail compensatory efforts to perform real-world functional movements. Hence, our robot can be used as an assistive device to enable prolonged arm use for users with upper limb impairments, especially for individuals living with ALS, for whom our robot improved the function of all upper limb joints in multiple degrees of freedom (Fig. 4D). The reduction in trunk compensation also provides evidence of the potential use of our robot as a rehabilitation tool for individuals post-stroke since over-reliance on compensatory strategies can limit motor recovery[37].

In line with the rehabilitation approach of offloading the arm weight to improve distal joint movements[4], our robot increased elbow and wrist ROM. The utility of our robot in improving joint function is higher than previous studies[1,24,38], who developed soft wearable shoulder robots to reduce muscular effort without improving joint function in individuals with upper limb impairments. Interestingly, compared to results from prior studies using elbow- and wrist-assisting robots, our shoulder-assisting robot achieved comparable improvements in elbow ROM and greater improvements in wrist ROM[39–41]. Although similar results showing that offloading arm weight in improving distal joint function have been demonstrated with in-clinic rigid robots[4], our robot offers a lightweight and portable solution to assist self-initiated functional arm use. However, to confirm the rehabilitative benefits of our robot, larger-scale clinical trials and longitudinal at-home studies are needed. Specifically, adaptively using the controller to tune the level of support (i.e., scale the output pressure

predicted by the human-robot hysteresis model) to match motor recovery can determine the robot's utility as a rehabilitation tool.

Despite promising results, our proposed method and implementation have several limitations. First, our sensing and intention detection strategy was designed for users with sufficient intact upper limb joint function to perform movements for training the IDMs. We therefore recruited individuals with mild to moderate levels of impairment (Supplementary Method S3), since we hypothesized they would benefit most from our control strategy. Future studies should consider a larger sample size with more diverse levels of impairment, which may require training the intention model with additional sensing modalities, such as sEMG or EEG, to capture smaller residual function. Second, our method focused on assisting only the shoulder joint; however, individuals with severe impairments oftentimes have difficulty using multiple joints. Future work could explore adding pneumatic actuators to directly assist the elbow, wrist, and hand, which may offer faster actuation due to lower torque required to move the joints. Third, the robot cannot be independently donned by individuals with upper limb impairments. In the future, further advancement in design is required to allow individuals with limited upper limb function to wear and use independently to validate the utility of our robot for independent use. Lastly, our control approach was not designed to model interactions with weighted objects or the effects of fatigue. While our at-home demonstration shows that the robot can allow individuals with impairments to lift weighted objects higher and for longer and that the robot can provide support in unconstrained ADLs, we observed in one participant with ALS that the level of support diminished post-fatigue. Modeling the effect of fatigue through training data augmentation or dynamic adjustment of the controller's hyperparameters (e.g., the level of support) over time could be explored in future studies.

We also note limitations in our evaluation. First, we were unable to quantify the accuracy of the IDMs during functional tasks beyond the initial UP and final DOWN movements, as we could not directly determine participants' intent to perform subtle shoulder elevation adjustments during fine object manipulation, such as repositioning a toothbrush or comb, or rotating a spoon or bottle. This made it challenging to distinguish between intentional changes and involuntary, impairment-induced movements. Our evaluation procedure aimed to overcome this challenge by including the shoulder elevated joint individuation tasks where we knew the users' intention to HOLD despite involuntary, impairment-induced movements. Second, we did not perform a systematic evaluation of the effect of different levels of accuracy for the IDMs, so we cannot quantify an exact threshold of acceptable accuracy. We found that 94.2% ± 2.0% was acceptable for achieving the improvements in upper limb movement quality and enabling improved performance in functional tasks. Future work evaluating the effect of accuracy on both users' movement quality and perception would be valuable.

Our control strategy for a portable soft wearable robot shows promise in fine-tuning the assistance to augment residual movement for individuals with two different types of upper limb impairments. We demonstrated that the new control strategy robustly provides assistance after small changes in the shoulder elevation/depression angle and short latency, while also improving transparency. In doing so, we showed it is possible to improve upper limb movement quality, opening up new opportunities for assistive technology to enhance performance during functional tasks and increasing the dose, quality and intensity of movement in upper limb motor rehabilitation.

Methods

High-level study design

We designed a multi-day study (2–3 days for each participant) to evaluate the efficacy of our proposed multimodal ML control strategy for a wearable shoulder robot that supports impaired upper limb movements. The proposed robot controller combines 1) personalized intention detection models (IDMs) that capture users' intended shoulder elevation direction and 2) a human-robot hysteresis model that captures the state dependent relationship between a user's arm pose and the actuator air pressure required for support.

On the first day of the study, we trained IDMs for 5 individuals post-stroke and 4 individuals living with ALS using robot-supported upper limb movement data during a guided session. The IDMs were trained to classify–in real-time–three directions of intended shoulder elevation: 1) lifting the arm (UP), 2) maintaining the arm elevation (HOLD), and 3) lowering the arm (DOWN). These three classes were selected for their simplicity, alignment with our control strategy, and demonstrated success in prior work[30].

On the second day of the study, we evaluated the efficacy of the trained IDMs in classifying the intended shoulder elevation direction to actuate the robot in parallel with the users' volitional movements. We also evaluated the efficacy of the combined IDM and human-robot hysteresis models on the robot's controller performance and upper limb movement quality. This evaluation was done by analyzing upper limb movements that required each participant to lift and lower their arm and perform joint movements while keeping their arm elevated, with and without being supported by the soft wearable robot.

On the third day of the study, a subset of the participants (one post-stroke and one living with ALS) completed evaluations at home to assess the effects of prolonged use and interactions with weighted objects in an unconstrained environment. Participants performed real (not simulated) activities of daily living in their homes before and after performing joint individuation and weight holding. The shoulder-elevated weight holding was performed with and without robot assistance.

Soft wearable robot hardware

The participants wore the soft wearable robot which our group designed to assist the shoulder movement[3]. In brief, the robot uses a textile-based, pneumatic actuator attached to a vest that can lift the arm about the shoulder joint (see Supplementary S1 for more details). All the electronics, valves, and an accumulator are housed inside a portable box (3 kg) that can be worn by the participants. The portable actuation box requires no external power supply or connection to a computer.

Compared to our group's previous work, we modified the robot's hardware to improve both state estimation and controller bandwidth. To enable motion intention detection, we developed soft compression sensors and integrated them into the shirt to capture the human-robot interaction. Building on previous research[42–44], these soft capacitive sensors detect changes in applied pressure by measuring variations in capacitance induced by compression in dielectric thickness (see Supplementary S2 for more details). To improve controller bandwidth, we reduced the pneumatic resistance introduced by proportional valves (Polaris, IQ Valves) which connect from the accumulator to the inflatable actuator by enabling input and output valves originally implemented for bimanual arm support to be used in parallel for unimanual support.

The IMUs and soft compression sensors streamed data to a microcomputer within the portable actuation box (Beaglebone Black Wireless, BeagleBoard.org Foundation) which is where the controller computation was performed, pneumatic valves and pump were sent commands, and controller data was logged. Hence, all controller computation was performed within the portable actuation box, with no external computer connection required. During in-lab evaluation, the actuation box was wired to synchronize logged data with optical motion capture and video. During at-home evaluation, the system was fully untethered. Due to the computational overhead required for performing the controller computation and the priority given to

maintaining a consistent rate for the controller, we observed some short periods of time where controller data was missing from the output log file. In our analysis, these missing periods of time in the controller were not imputed or interpolated and were instead excluded from the controller related analysis.

Participants

We recruited 9 individuals with upper limb impairments (5 individuals post-stroke and 4 individuals living with ALS) to participate in the study. All 9 participants performed the first two days of the study, and 2 performed the third day at-home. The demographic, anthropometric, and functional level found from clinical assessment measures for each participant are compiled in Table 1. The participant inclusion and exclusion criteria are provided in Supplementary S3. One participant post-stroke and three participants living with ALS were wheelchair users and could not walk independently. All the aspects of the study adhered to the guidelines described in the Declaration of Helsinki and were approved by the institutional review board (IRB) of Harvard Medical School (IRB No. 13-3418).

Experimental procedure to acquire data to train personalized IDMs

We acquired training data during a guided session where we asked the participants to perform a series of dynamic and quasistatic shoulder elevation movements (Fig. 1C, Supplementary Table S1). These tasks are described in detail in Supplementary S4. During the training, the actuator supported the paretic (individuals post-stroke) or weaker arm (individuals living with ALS).

Design of the intention detection models

Input data. Considering that we trained and evaluated the IDM on separate days, we selected the input features for the IDMs that had minimal effect due to changes in sensor placement caused by donning/doffing the robot. Specifically, joint velocities and changes in compression of the soft compression sensors attached to the human-robot interaction surfaces were selected as input features for the IDM since these signals captured residual movement while being minimally sensitive to the sensors' exact placement after redonning the robot. In total, we selected six input signals to calculate the features to train the IDMs: 1) shoulder elevation/depression velocity, 2) shoulder horizontal abduction/adduction velocity, 3) elbow flexion/extension velocity, 4) derivative of torso soft compression sensor signal, 5) derivative of medial upper arm soft compression sensor signal, and 6) derivative of lateral upper arm soft compression sensor signal.

These signals were first smoothened by applying a short moving average filter with a 20 ms window. To minimize the effect of noise in the sensor data and learn patterns from temporal trends, we included data from the current timestep and acquired historical data from the preceding 50 ms (5 control iterations at 100 Hz). In total, the IDMs included 36 input features that were used to perform each inference: the 6 current features and 5×6 historical features. This window size and the number of features were selected to balance trade-offs related to the sensitivity of the model to noise, the latency in performing the inference, and the amount of training data required.

Model architecture. We chose the IDM architecture as a fully connected neural network with two dense layers (20, 10 neurons) and ReLU as the activation function. Regularization was applied to both layers to prevent overfitting. Specifically, L1 regularization was used with a regularization strength of 0.00001 to penalize large weights in the neural network. A softmax layer was used to output confidence thresholds for the predictions in the three classes (UP, HOLD, and DOWN). The simple architecture for the model was selected based on pilot testing, to ensure that sufficient patterns in data were captured while keeping the time to perform inference sufficiently fast at every control iteration to not cause delays in controller response.

Training. The training data was windowed with a stride of 10 ms so that each window contained the 36 features that were input to the neural network. 20% of the training windows (selected at random) were held apart for validation during training. To address the imbalance present in our training data (with windows labeled as HOLD being more common than those labeled as UP or DOWN), we weighted the loss function used during training by the ratio of windows within each class present in each participant's training data. To showcase the models' generalizability across days–since retraining the IDM each time the robot is worn is impractical–we trained the IDMs on a separate day from when the model was evaluated as part of the multimodal ML controller.

Real-time inference. After running the training for 30 epochs using TensorFlow, the trained model was then deployed on the robot as a TensorFlow Lite[45] model using the Edge Impulse DSP and Inferencing SDK[46] which enabled the intention detection to run in real-time as the participants moved. To smooth the predictions from the model and avoid undesired frequent transitions between IDM classes, we applied a short moving average filter with a window of 20 ms to the output confidence of each class. When the model was run in real-time, the output confidences were used to classify the current intention state as either UP, HOLD, or DOWN. UP/HOLD/DOWN Confidence Thresholds were hyperparameters controlling the confidence levels required to assign class labels at runtime. The order of precedence for assigning class labels based on the Confidence Thresholds was DOWN, followed by UP, and finally HOLD. If none of the confidence thresholds were passed, the controller defaulted to the HOLD state.

Human-robot hysteresis model

To determine the actuator pressure that was necessary for support while a user performed dynamic upper limb movement, we built on our previous work[23] modeling the hysteresis in the human-robot system with a Preisach model. This hysteresis model allowed us to capture the relationship of the actuator air pressure required to support the arm at a given shoulder elevation angle, which is specific to each person. The variability within participants on separate days (Supplementary Fig. S2) indicates that there was a need for performing this calibration each time the robot was donned, unlike the IDMs which were shown to generalize across days. We modified the model introduced in our previous work[23] to account for the impact of flexing the elbow on torque required to support the shoulder. We have described the details of this improved human-robot hysteresis model in S5.

Multimodal ML controller design

We combined the intention detection and hysteresis models to create an integrated controller that enabled transparent gravity compensation control during HOLD, and tunable additional support during UP and DOWN. Figure 3A illustrates the main principle for combining the predictions from IDMs (UP, HOLD, or DOWN) and predictions from the hysteresis model for pressure required for gravity compensation.

In the UP and DOWN states, the estimated shoulder elevation angle was offset by a constant angle, the UP/DOWN Angle Shift parameter, in the direction of movement. For example, if the DOWN Angle Shift parameter were set to 5°, whenever the controller was in the DOWN state, the robot would command the actuator pressure required to support the current estimated elevation angle minus 5°. In this way, the robot anticipated a user's future movement and reacted quickly whenever a person's intention was to move in a particular direction.

In the HOLD state, the controller's objective was to maintain gravity compensation support while maximizing the transparency of

the system for future movements. To address the objective of maintaining transparency, we used the hysteresis model to predict the minimum necessary pressure to support the elevation angle ±1° when the user first entered the HOLD state. The small tolerance on angle (±1°) oftentimes allowed for significantly reduced pressure in the HOLD state while still maintaining support of the arm, and by reducing the pressure, the actuator was more transparent to future downward movement. For example, if a user lifted their arm to 90° and then stopped (entering the HOLD state), the actuator was allowed to reduce the pressure so that the actuator provided the pressure to support 89°. This small change in angle enabled significant reductions in the actuator pressure (example in Supplementary Fig. S5). Additional details about the minimum necessary pressure implementation are described in Supplementary S6.

A diagram of the full controller architecture is shown in Supplementary Fig. S4, which shows how the user's residual movement is measured by the wearable sensors, passed into the hysteresis model and IDM, and the pressure in the actuator is set at each control iteration by the low-level pneumatic controller described in Supplementary S7.

Experimental procedure for in-lab evaluation

After calibrating the human-robot hysteresis model and tuning the personalized IDM to each participant's preference (see Supplementary S8 for details and Supplementary Table S3 for each participant's controller hyperparameters), we evaluated the accuracy of the IDMs and their effect on the robot's real-time controller and upper limb movement quality during two categories of tasks: 1) joint individuation and 2) functional tasks (Supplementary Fig. S7).

The joint individuation tasks consisted of isolated shoulder, elbow, and wrist joint movements and forearm movements. Shoulder joint movements were performed in all 3 degrees of freedom, while only flexion/extension movements were performed for elbow and wrist joints, and pronation/supination movement for the forearm. Besides shoulder elevation/depression movements, the rest of the movements were performed while keeping the arm elevated at a steady 90°. We asked the participants to hold between the lifting (UP) and lowering (DOWN) of the arm. For shoulder elevated joint movements, we asked the participants to keep their arm elevated at 90° (HOLD) and perform back-and-forth joint movements (3 repetitions), while holding before changing the direction of movement (e.g., elbow extension, hold, and then elbow flexion).

For functional tasks, we asked the participants to perform four simulated activities of daily living (ADLs): brushing teeth, combing hair, drinking, and eating. Specifically, we instructed the participants to lift their arm, manipulate an object to simulate performing an ADL (e.g. brushing teeth using a toothbrush), and lower their arm. The participants were asked to hold in place after completing a motion cue. A single investigator guided each participant's movement by providing instructions on when to initiate and terminate movements.

The participants performed all the tasks 3 times each under two conditions: the robot turned on (ON) and off (OFF) in a randomized order. Additionally, we asked participants to perform the shoulder elevation movements with a baseline gravity compensation controller to compare the effectiveness with the multimodal ML controller (see Results). An optical motion capture system was used to record upper limb movements by tracking the retro-reflective markers attached to the key anatomical landmarks outlined in S9. The motion capture system was time-synced with a camcorder to record videos that were used to identify UP, DOWN, and HOLD intentions.

Controller evaluation. To assess the controller during the evaluation on the second day of the experiment, we calculated metrics to quantify the performance of both the IDMs and integrated controller. For the IDMs, we evaluated their accuracy across movements, generalizability across participants, and responsiveness to changes in intention. For the integrated, multimodal ML controller, we evaluated the controller's responsiveness, response during IDM misclassifications, ability to estimate the minimum necessary pressure, and the transparency of the robot when lowering. We define these metrics in the Results section and provide more detailed descriptions of their calculation in Supplementary S10. Data analysis related to the controller response was performed using Python version 3.10.12 and C++14.

Upper limb movement quality evaluation

We first filtered the raw positions of the retro-reflective markers using a zero-lag, fourth-order low-pass Butterworth filter with a cut-off frequency of 10 Hz. Then, we built a four-segment (hand, forearm, upper arm of the shoulder-supported side, and torso) using a biomechanical modeling software, Visual 3D (Visual 3D v6TM, C-Motion, Inc., Maryland, USA), to calculate kinematics metrics. All the movement quality metrics calculation was performed in MATLAB (Version R2024a)

Joint function. We evaluated the joint function by calculating the shoulder elevation/depression, abduction/adduction, and internal/external rotation; elbow and wrist flexion/extension; and forearm supination/pronation ROMs. We selected ROMs as a metric to evaluate upper limb movement quality because larger ROMs increase the capacity to perform more ADLs, leading to greater functional independence, and prevent contractures that could limit function and increase pain[47–50]. These ROMs were calculated by taking the absolute difference between the maximum and minimum values during the upper limb joint movements.

Trunk compensation. We evaluated the trunk compensation by calculating the 3D trunk center of mass (COM) displacement, separately for UP and DOWN during isolated shoulder elevation of the individuation tasks and functional tasks. We selected trunk compensation as a metric to evaluate upper limb movement quality because increased reliance on trunk to move the hand leads to reduction in residual capacity of upper limb joints, accelerating functional decline and hampering motor recovery[51–53]. The 3D trunk COM displacement was quantified as the sum of the time series magnitude of displacement of the trunk in X ($Trunk_{COMx}$), Y ($Trunk_{COMy}$), and Z ($Trunk_{COMz}$) directions such that,

$$Trunk_{disp} = \sum_{n=1}^{k} \sqrt{\begin{array}{l}(Trunk_{COMx}(i) - Trunk_{COMx}(i-1))^2 + \\ (Trunk_{COMy}(i) - Trunk_{COMy}(i-1))^2 + \\ (Trunk_{COMz}(i) - Trunk_{COMz}(i-1))^2\end{array}} \quad (1)$$

where i = 2, ..., k, and k is the length of the time series of Trunk COM.

Hand path efficiency and smoothness. We calculated hand path efficiency and smoothness using the 3D hand COM trajectory, separately during UP and DOWN for individuation tasks and functional tasks. We selected hand path efficiency and smoothness as metrics to evaluate movement quality because smooth and straight end-effector (hand) movement is required to perform ADLs in a skilled and well-coordinated manner[54,55]. Additionally, blending of fragmented hand movement while being able to move the hand in a straight line between two points in space is an indicator of recovery of upper limb function after motor impairment[56,57].

We quantified the path efficiency by calculating the hand-path-ratio (HPR) as,

$$HPR = \frac{D_{actual}}{D_{straight}} - 1 \quad (2)$$

where D_{actual} is the distance traveled by the 3D hand COM and $D_{straight}$ is the shortest possible distance between movement initiation and termination. Hence, HPR = 0 indicates that the hand traveled in the most efficient path; values closer to 0 indicate high hand path efficiency.

We calculated the path smoothness by calculating the spectral arc length (SPARC)[58], which is the negative arc length of the Fourier magnitude spectrum of the 3D resultant velocity of the hand COM trajectories. Larger SPARC values indicate higher smoothness. We calculated HPR and SPARC values separately for UP and DOWN movements, and during individuation and functional tasks.

We also compared all the movement quality metrics separately for the two participant subgroups based on the cause of impairment (Stroke and ALS) and compared the difference between the two subgroups (see Supplementary S11).

Experimental procedure for at-home demonstration

Two participants wore the robot and completed the human-robot hysteresis calibration (using the IDM model trained on the first day of the study) in their homes. They then performed ADLs (eating from a bowl with a spoon, drinking from a cup, and brushing teeth) using their own utensils and objects. Participants chose to sit or stand for these tasks based on their typical routines.

After completing the ADLs with the controller ON and OFF, participants performed a timed weight holding task. Wearing a wrist weight, they attempted to lift their arms to 90° elevation following flexion and abduction movements under both controller conditions. The maximum hold time was 2 minutes. The post-stroke participant used a 1.13 kg weight, and the participant with ALS used a 0.23 kg weight, both self-selected to ensure task feasibility. Afterwards, participants performed shoulder-elevated joint individuation tasks with the controller ON and OFF to simulate prolonged arm use of multiple joints.

At the end of the experiment, participants repeated the ADLs with the controller ON and OFF to assess the impact of prolonged use on robot performance. The ON and OFF conditions were randomized throughout the experiment. Before each set of ADLs, the therapist asked the participant to rate their fatigue using the Borg CR–10 scale[59]. The FMA-UE and ALSFRS-R were also administered to confirm participants' functional ability had not significantly changed since IDM training (1 year prior for the participant living with ALS, 6 months prior for the participant post-stroke).

We provide detailed descriptions of the metrics we calculated from the experiments in Supplementary S11. Unlike the second day in-lab evaluation, we lacked precisely time-synced motion capture and video. Although we recorded approximately synced videos, the absence of exact synchronization made precise timing and accuracy metrics unreliable. We therefore focused on more coarse metrics of performance such as average IMU-estimated elevation angle and actuator pressure during the tasks and duration during timed weight holding.

Statistical analysis

All the results for upper limb movement quality are presented as mean ± standard error. We evaluated the significant differences in the upper limb movement quality metrics between ON and OFF conditions across all participants, and separately for two participant groups using either two-tailed, paired *t*-test or two-tailed Wilcoxon-signed rank test. Additionally, we used paired *t*-tests to compare the peak compression force, peak shoulder elevation, and peak actuator pressure between the baseline and multimodal ML controller to assess the robot's transparency during lowering of the arm. Finally, we used either a two-tailed, independent *t*-test or two-tailed Mann–Whitney U test to compare the results of upper-limb movement quality change under ON condition with respect to OFF condition between the two participant subgroups. An independent *t*-test and paired *t*-test were selected if the values for each of the movement quality metrics were normally distributed, assessed using the Shapiro–Wilk test. The level of statistical significance was set at $p < 0.05$. All statistical analysis was performed using SPSS (Version 29.0)

Data availability

All data supporting the findings of this study are available in the main text and supplementary materials. The supplementary information includes the data needed to reproduce all figures and evaluate the results. Additional details can be requested from the corresponding author. Source data are provided with this paper.

Code availability

The C++ file with the code for the multimodal ML controller is provided as supplementary material (Supplementary Code 1). To run the code, additional libraries for specific wearable robot hardware are required. Prior work and additional resources have been referenced but not included in the code as they are not the original contributions of this work. Additional specifics regarding the controller code can be provided upon reasonable request to the corresponding author.

References

1. Georgarakis, A.-M., Xiloyannis, M., Wolf, P. & Riener, R. A textile exomuscle that assists the shoulder during functional movements for everyday life. *Nat. Mach. Intell.* **4**, 574–582 (2022).
2. Lee, J. et al. Intelligent upper-limb exoskeleton integrated with soft bioelectronics and deep learning for intention-driven augmentation. *npj Flex. Electron.* **8**, 11 (2024).
3. Proietti, T. et al. Restoring arm function with a soft robotic wearable for individuals with amyotrophic lateral sclerosis. *Sci. Transl. Med.* **15**, eadd1504 (2023).
4. Sukal, T. M., Ellis, M. D. & Dewald, J. P. Shoulder abduction-induced reductions in reaching work area following hemiparetic stroke: neuroscientific implications. *Exp. Brain Res.* **183**, 215–223 (2007).
5. Perry, B., Sivak, J. & Stokic, D. Providing unloading by exoskeleton improves shoulder flexion performance after stroke. *Exp. Brain Res.* **239**, 1539–1549 (2021).
6. Ellis, M. D., Sukal-Moulton, T. & Dewald, J. P. Progressive shoulder abduction loading is a crucial element of arm rehabilitation in chronic stroke. *Neurorehabilit. Neural Repair.* **23**, 862–869 (2009).
7. Parnandi, A. et al. Data-driven quantitation of movement abnormality after stroke. *Bioengineering* **10**, 648 (2023).
8. Gantenbein, J., Dittli, J., Meyer, J. T., Gassert, R. & Lambercy, O. Intention detection strategies for robotic upper-limb orthoses: a scoping review considering usability, daily life application, and user evaluation. *Front. Neurorobotics* **16**, 815693 (2022).
9. Capsi-Morales, P. et al. Functional assessment of current upper limb prostheses: an integrated clinical and technological perspective. *Plos one* **18**, e0289978 (2023).
10. Losey, D. P., McDonald, C. G., Battaglia, E. & O'Malley, M. K. A review of intent detection, arbitration, and communication aspects of shared control for physical human–robot interaction. *Appl. Mech. Rev.* **70**, 010804 (2018).
11. Hudgins, B., Parker, P. & Scott, R. N. A new strategy for multifunction myoelectric control. *IEEE Trans. Biomed. Eng.* **40**, 82–94 (1993).
12. Englehart, K. & Hudgins, B. A robust, real-time control scheme for multifunction myoelectric control. *IEEE Trans. Biomed. Eng.* **50**, 848–854 (2003).
13. McDonald, C. G., Sullivan, J. L., Dennis, T. A. & O'Malley, M. K. A myoelectric control interface for upper-limb robotic rehabilitation following spinal cord injury. *IEEE Trans. Neural Syst. Rehabilit. Eng.* **28**, 978–987 (2020).
14. Zia ur Rehman, M. et al. Multiday EMG-based classification of hand motions with deep learning techniques. *Sensors* **18**, 2497 (2018).

15. Hoppe-Ludwig, S. et al. Usability, functionality, and efficacy of a custom myoelectric elbow-wrist-hand orthosis to assist elbow function in individuals with stroke. *J. Rehabilit. Assist. Technol. Eng.* **8**, 20556683211035057 (2021).
16. Chiaradia, D., Xiloyannis, M., Antuvan, C. W., Frisoli, A. & Masia, L. Design and embedded control of a soft elbow exosuit. In 2018 *IEEE international conference on soft robotics (RoboSoft)*. 565–571 (IEEE, 2018).
17. Zhou, Y. M., Hohimer, C., Proietti, T., O'Neill, C. T. & Walsh, C. J. Kinematics-based control of an inflatable soft wearable robot for assisting the shoulder of industrial workers. *IEEE Robot. Autom. Lett.* **6**, 2155–2162 (2021).
18. Lessard, S. et al. A soft exosuit for flexible upper-extremity rehabilitation. *IEEE Trans. Neural Syst. Rehabilit. Eng.* **26**, 1604–1617 (2018).
19. Sasaki, D., Noritsugu, T., Takaiwa, M. & Kataoka, Y. Development of pneumatic wearable power assist device for human arm "ASSIST". In *Proceedings of the JFPS International Symposium on Fluid Power*, 202–207 (The Japan Fluid Power System Society, 2005).
20. Zimmermann, Y., Forino, A., Riener, R. & Hutter, M. ANYexo: a versatile and dynamic upper-limb rehabilitation robot. *IEEE Robot. Autom. Lett.* **4**, 3649–3656 (2019).
21. Jones, C. L., Wang, F., Morrison, R., Sarkar, N. & Kamper, D. G. Design and development of the cable actuated finger exoskeleton for hand rehabilitation following stroke. *IEEE ASME Trans. Mechatron.* **19**, 131–140 (2012).
22. Asbeck, A. T., De Rossi, S. M., Holt, K. G. & Walsh, C. J. A biologically inspired soft exosuit for walking assistance. *Int. J. Robot. Res.* **34**, 744–762 (2015).
23. McCann, C., Arnold, J., Lehmacher, C., Bertoldi, K. & Walsh, C. On-body textile hysteresis estimation for personalized physical human-robot interaction. *Int. J. Robot. Res.* https://doi.org/10.1177/02783649251358840 (2025).
24. Simpson, C. et al. Upper extremity exomuscle for shoulder abduction support. *IEEE Trans. Med. Robot Bionics* **2**, 474–484 (2020).
25. Nam, C. et al. An exoneuromusculoskeleton for self-help upper limb rehabilitation after stroke. *Soft Robot.* **9**, 14–35 (2022).
26. Murphy, M. A., Willén, C. & Sunnerhagen, K. S. Kinematic variables quantifying upper-extremity performance after stroke during reaching and drinking from a glass. *Neurorehabilit. Neural Repair.* **25**, 71–80 (2011).
27. Unger, T. et al. Upper limb movement quality measures: comparing IMUs and optical motion capture in stroke patients performing a drinking task. *Front. Digital Health* **6**, 1359776 (2024).
28. Lu, Z., Tong, K. -y, Zhang, X., Li, S. & Zhou, P. Myoelectric pattern recognition for controlling a robotic hand: a feasibility study in stroke. *IEEE Trans. Biomed. Eng.* **66**, 365–372 (2018).
29. Park, S. et al. Multimodal sensing and interaction for a robotic hand orthosis. *IEEE Robot. Autom. Lett.* **4**, 315–322 (2018).
30. Choi, A., Kim, T. H., Chae, S. & Mun, J. H. Improved transfer learning for detecting upper-limb movement intention using mechanical sensors in an exoskeletal rehabilitation system. In *IEEE Transactions on Neural Systems and Rehabilitation Engineering* (IEEE, 2024).
31. Lotti, N. et al. Adaptive model-based myoelectric control for a soft wearable arm exosuit: a new generation of wearable robot control. *IEEE Robot. Autom. Mag.* **27**, 43–53 (2020).
32. Yap, H. K., Lim, J. H., Nasrallah, F. & Yeow, C.-H. Design and preliminary feasibility study of a soft robotic glove for hand function assistance in stroke survivors. *Front. Neurosci.* **11**, 547 (2017).
33. Cirstea, M. & Levin, M. F. Compensatory strategies for reaching in stroke. *Brain* **123**, 940–953 (2000).
34. Kadivar, Z., Beck, C. E., Rovekamp, R. N. & O'Malley, M. K. Single limb cable driven wearable robotic device for upper extremity movement support after traumatic brain injury. *J. Rehabilit. Assist. Technol. Eng.* **8**, 20556683211002448 (2021).
35. Wu, C. -y., Yang, C. -l., Chen, M. -d, Lin, K. -c. & Wu, L. -l. Unilateral versus bilateral robot-assisted rehabilitation on arm-trunk control and functions post stroke: a randomized controlled trial. *J. Neuroeng. Rehabilit.* **10**, 1–10 (2013).
36. Hsieh, Y. -w et al. Sequencing bilateral robot-assisted arm therapy and constraint-induced therapy improves reach to press and trunk kinematics in patients with stroke. *J. Neuroeng. Rehabilit.***13**, 1–9 (2016).
37. Levin, M. F., Kleim, J. A. & Wolf, S. L. What do motor "recovery" and "compensation" mean in patients following stroke?. *Neurorehabilit. Neural Repair.* **23**, 313–319 (2009).
38. Simpson, C. S., Okamura, A. M. & Hawkes, E. W. Exomuscle: An inflatable device for shoulder abduction support. In *2017 IEEE International Conference on Robotics and Automation (ICRA)*. 6651–6657 (IEEE, 2017).
39. Noronha, B. et al. Soft, lightweight wearable robots to support the upper limb in activities of daily living: a feasibility study on chronic stroke patients. *IEEE Trans. Neural Syst. Rehabilit. Eng.* **30**, 1401–1411 (2022).
40. Young, H., et al. Air efficient soft wearable robot for high-torque elbow flexion assistance. In *2023 International Conference on Rehabilitation Robotics (ICORR)*. 1–6 (IEEE, 2023).
41. Nijenhuis, S. M., Prange, G. B., Stienentt, A., Buurke, J. & Rietman, J. S. Direct effect of a dynamic wrist and hand orthosis on reach and grasp kinematics in chronic stroke. In 2015 *IEEE international conference on rehabilitation robotics (ICORR)*. 404–409 (IEEE, 2015).
42. Atalay, O., Atalay, A., Gafford, J. & Walsh, C. A highly sensitive capacitive-based soft pressure sensor based on a conductive fabric and a microporous dielectric layer. *Adv. Mater. Technol.* **3**, 1700237 (2018).
43. Jin, Y., et al. Soft sensing shirt for shoulder kinematics estimation. In *2020 IEEE International Conference on Robotics and Automation (ICRA)*, 4863–4869 (IEEE, 2020).
44. Meyer, J., Arnrich, B., Schumm, J. & Troster, G. Design and modeling of a textile pressure sensor for sitting posture classification. *IEEE Sens. J.* **10**, 1391–1398 (2010).
45. Tensorflow Lite, https://ai.google.dev/edge/litert (accessed 2024–2025).
46. Edge Impulse, https://github.com/edgeimpulse/inferencing-sdk-cpp (accessed 2024–2025).
47. Oosterwijk, A. M., Nieuwenhuis, M. K., van der Schans, C. P. & Mouton, L. J. Shoulder and elbow range of motion for the performance of activities of daily living: a systematic review. *Physiother. Theory Pract.* **34**, 505–528 (2018).
48. Beebe, J. A. & Lang, C. E. Active range of motion predicts upper extremity function 3 months after stroke. *Stroke* **40**, 1772–1779 (2009).
49. Majmudar, S., Wu, J. & Paganoni, S. Rehabilitation in amyotrophic lateral sclerosis: why it matters. *Muscle Nerve* **50**, 4–13 (2014).
50. Paganoni, S., Karam, C., Joyce, N., Bedlack, R. & Carter, G. T. Comprehensive rehabilitative care across the spectrum of amyotrophic lateral sclerosis. *NeuroRehabilitation* **37**, 53–68 (2015).
51. Jones, T. A. Motor compensation and its effects on neural reorganization after stroke. *Nat. Rev. Neurosci.* **18**, 267–280 (2017).
52. Alaverdashvili, M., Foroud, A., Lim, D. H. & Whishaw, I. Q. Learned baduse" limits recovery of skilled reaching for food after forelimb motor cortex stroke in rats: a new analysis of the effect of gestures on success. *Behav. Brain Res.* **188**, 281–290 (2008).
53. Lum, P. S. et al. Gains in upper extremity function after stroke via recovery or compensation: potential differential effects on amount of real-world limb use. *Top. Stroke Rehabilit.* **16**, 237–253 (2009).
54. Engdahl, S. M. & Gates, D. H. Reliability of upper limb movement quality metrics during everyday tasks. *Gait Posture* **71**, 253–260 (2019).

55. Hogan, N. & Sternad, D. Sensitivity of smoothness measures to movement duration, amplitude, and arrests. *J. Mot. Behav.* **41**, 529–534 (2009).
56. Rohrer, B. & Hogan, N. Avoiding spurious submovement decompositions II: a scattershot algorithm. *Biol. Cybern.* **94**, 409–414 (2006).
57. Osu, R. et al. Quantifying the quality of hand movement in stroke patients through three-dimensional curvature. *J. Neuroeng. Rehabilit.***8**, 1–14 (2011).
58. Balasubramanian, S., Melendez-Calderon, A., Roby-Brami, A. & Burdet, E. On the analysis of movement smoothness. *J. Neuroeng. Rehabilit.* **12**, 1–11 (2015).
59. Borg, G. Psychophysical scaling with applications in physical work and the perception of exertion. *Scand. J. Work Environ. Health*, **16**, 55–58 (1990).

Acknowledgements

We thank Andrew Chin, Elizabeth L. Suitor, Fivos Kavassalis, Jacqueline Villalobos, Tom Hoang, Umut S. Civici, Farasoa D. Rajaona, Ada Huang, Kiley Baker, Keysa Garcia, Sarah Taylor, Dionna O. Roberts Williams, and the study participants for their contributions to this work. This work is supported by National Science Foundation award under Grant No. 2236157 and 2345107 (D.L. and C.J.W.), the National Science Foundation Graduate Research Fellowship under Grant No. DGE 2140743 (J.A.), the Raj Bhattacharyya and Samantha Heller Assistive Technology Initiative Fund (C.J.W.), and Harvard University John A. Paulson School of Engineering and Applied Sciences (C.J.W.).

Author contributions

Conceptualization: J.A., P.P., and C.J.W.; Methodology: J.A., P.P., Y.J., D.P.-E., C.M.M., C.L., J.P.B., T.C., and C.J.W.; Software: J.A., P.P., Y.J., D.P.-E., C.M.M., C.L., T.L.; Validation: J.A., P.P., Y.J., and C.J.W; Formal Analysis: J.A., P.P., and Y.J.; Investigation: J.A., P.P., Y.J., J.P.B., T.L., K.M.B., S.C., L.B., K.R., and C.J.W.; Resources: J.A., P.P., J.P.B., K.M.B., S.C., L.B., K.R., S.P., D.L., and C.J.W.; Data Curation: J.A., P.P., and Y.J.; Visualization: J.A., P.P., and Y.J.; Writing—original draft: J.A., P.P., Y.J., D.P.-E., C.M.M., and C.J.W.; Writing—review and editing: All authors; Supervision: S.P., D.L., and C.J.W.; Project Administration: J.A., P.P., and C.J.W.; Funding Acquisition: D.L. and C.J.W.

Competing interests

C.J.W. is a co-inventor of U.S. patent US 12,097,159 filed by Harvard University that describes the inflatable soft robotic components tested in this study. C.J.W., J.A., C.M.M., and C.L. are co-inventors of U.S. patent application US 2024/043077 filed by Harvard University that describes the control strategy tested in this study. The remaining authors declare no competing interests.

Additional information

Supplementary information The online version contains supplementary material available at https://doi.org/10.1038/s41467-025-62538-8.

Correspondence and requests for materials should be addressed to Conor J. Walsh.

Peer review information *Nature Communications* thanks Marcia O'Malley, and the other, anonymous, reviewer(s) for their contribution to the peer review of this work. A peer review file is available.